*Science World Journal Vol. 21(No 3) 2026* https://dx.doi.org/10.4314/swj.v21i3.10
*www.scienceworldjournal.org*
*ISSN: 1597-6343 (Online), ISSN: 2756-391X (Print)*
*Published by Faculty of Science, Kaduna State University*

Full Length Research Article

# TRANSIENT MHD DOUBLE-DIFFUSIVE FREE CONVECTION OF AG-CU HYBRID NANOFLUIDS OVER AN INCLINED POROUS PLATE WITH THERMAL RADIATION AND SORET-DUFOUR EFFECTS

*[1]J.O. Ajilore, [2]O.K. Onanuga, [3]T.O. Ogunjare, [1]I.A. Idowu

[1]Department of Mathematical Science, Lagos State University of Science and Technology, Ikorodu, Nigeria
[2]Department of Physical Sciences, Lagos State University of Science and Technology, Ikorodu, Nigeria
[3]Department of Mathematics, Yaba College of Technology, Yaba, Lagos, Nigeria

*Corresponding Author Email Address: joshua104u@yahoo.com

**ABSTRACT**
The study explores the transient MHD double-diffusive free-convective transport of an Ag-Cu/water-hybridized nanofluid along an inclined porous plate, accounting for heat generation/absorption, thermal radiation, Soret and Dufour effects, and chemical reaction. The formulated mathematical model for the governing equations of momentum, energy, and concentration is subject to initial and boundary conditions. Rosseland's diffusion approximation is used to describe the radiative heat transfer, while the effective thermophysical properties of the hybrid nanofluid are considered. The resulting partial differential equations are transformed into dimensionless form using suitable similarity variables and solved using an explicit finite-difference scheme. A parametric investigation is conducted to examine the effects of fluid parameters on velocity, heat, and species distributions, as well as on the skin friction, Nusselt, and Sherwood numbers. The results show that the rising magnetic field term and porous medium resistance reduce the fluid velocity, whereas stronger thermal and solutal buoyancy forces significantly promote the flow. Thermal radiation and the Dufour effect increase the thickness of the thermal boundary layer. The concentration boundary layer improves with increasing Soret number but worsens with increasing Schmidt number. The findings provide valuable insights into the thermal management and transport characteristics of hybrid nanofluids in advanced heat-transfer devices.

**Keywords:** Ag-Cu/water-hybridized nanofluid; Thermal radiation; Double diffusion fluid; Free convection; Soret-Dufour Effects**.**

## INTRODUCTION

The efficient transport of heat and mass is fundamental to numerous engineering systems, including energy conversion devices, chemical reactors, electronic cooling technologies, biomedical equipment, geothermal systems, and manufacturing processes. Conventional heat transfer fluids such as water, ethylene glycol, and oils typically exhibit low thermal conductivity, which limits their performance in advanced thermal management applications. To overcome this limitation, nanofluids, engineered by dispersing nanoparticles in conventional base fluids, have attracted significant attention for their superior thermal transport capabilities. Since the pioneering work of Choi (1995), nanofluids have become an active area of research due to their ability to enhance heat transfer without substantial modifications to existing thermal systems. Numerous experimental and numerical investigations have demonstrated that incorporating metallic or metal-oxide nanoparticles into base fluids significantly improves thermal conductivity, convective heat transfer, and overall energy efficiency [Choi(1995), Lee *et al* (1999), Hong *et al* (2006), Mustafa *et al* (2015), Azmi (2016), Khan & Pop (2010), Mahanthesh *et al* (2016), Hayat& Nadeem (2017).

In many industrial processes, heat and mass transfer occur simultaneously rather than independently. Such coupled transport phenomena become even more significant when concentration and temperature gradients interact through cross-diffusion. These interactions are commonly represented by the Soret (thermal diffusion) and Dufour (diffusion-thermo) effects. The Soret effect describes species migration induced by temperature gradients, whereas the Dufour effect accounts for heat flux generated by concentration gradients. These mechanisms are particularly important in isotope separation, petroleum refining, geothermal reservoirs, polymer processing, chemical vapor deposition, drying technologies, combustion systems, food preservation, and pharmaceutical manufacturing. Ignoring these cross-diffusion effects may result in inaccurate prediction of transport behavior in many practical engineering applications. Several researchers have investigated different aspects of MHD nanofluid transport. Balla *et al*. (2020) examined chemically reacting bio-convective nanofluid flow in porous media containing oxytactic microorganisms. Shamshuddin *et al*. (2021) studied the thermal and concentration characteristics of Cu/CuO nanofluids over a nonlinear stretching surface with heat generation and chemical reaction. Puneeth *et al*. (2021) analyzed radiative hybrid nanofluid bio convection over a thin needle, considering homogeneous and heterogeneous reactions. Additional investigations have explored chemically reacting MHD nanofluid flows with various geometries and boundary conditions [Shamshuddin *et al. (2021), Arshad et al. (2021), Biswas et al. (2022), Shamshuddin et al. (2023), Reddy et al. (2022)]*. Thermal radiation effects on MHD nanofluid transport have also been extensively investigated by Roja & Gireesha (2020), Kumar *et al*. (2021), Reddy *et al*. (2022), and several other researchers [Suresh *et al* (2023), Shamshuddin *et al* (2023), Salawu *et al* (2023), Reddy & Goud (2023). Likewise, studies by Singha *et al*. (2021), Padmaja & Kumar (2022), Siddique *et al* (2022), Haritha *et al* (2023), and Raghunath (2023) demonstrated the importance of Soret and Dufour effects in coupled heat and mass transfer problems.

Despite these significant contributions, limited attention has been devoted to the simultaneous investigation of transient MHD free convection of Ag–Cu hybrid nanofluids over an inclined porous plate, accounting for the combined effects of thermal radiation, chemical reaction, porous medium resistance, heat generation, and coupled Soret–Dufour effects. Most existing studies consider only a subset of these interacting physical mechanisms or focus primarily on single-component nanofluids. The combined influence of these parameters remains insufficiently understood despite its importance in many industrial applications. Motivated by these research gaps, the present study develops a comprehensive mathematical model that describes transient double-diffusive magnetohydrodynamic free-convective transport of an Ag–Cu/water hybrid nanofluid over an inclined porous plate. The outcomes of this study provide useful physical insights for the design and optimization of thermal systems involving electrically conducting hybrid nanofluids in porous media, with applications in energy conversion, electronic cooling, chemical processing, geothermal engineering, nuclear systems, pharmaceutical manufacturing, and advanced thermal management technologies.

## RESEARCH GAP

Despite the growing interest in Ag–Cu hybrid nanofluids due to their superior thermal conductivity, there remains a lack of comprehensive studies examining transient double-diffusive free convection over an inclined porous plate under the simultaneous influence of magnetohydrodynamics (MHD), thermal radiation, heat generation/absorption, chemical reaction, porous medium resistance, and the coupled Soret–Dufour effects. Existing studies generally neglect one or more of these interacting mechanisms, making it difficult to understand their combined influence on momentum, thermal energy, and species transport.

## RESEARCH NOVELTY

The novelty of this study lies in the development of a comprehensive transient mathematical model that integrates multiple interacting transport mechanisms governing the flow and heat-transfer characteristics of an Ag–Cu/water hybrid nanofluid over an inclined porous plate. While previous studies have examined magnetohydrodynamic (MHD) nanofluid flows, thermal radiation, porous media, chemical reactions, or Soret–Dufour effects individually or in limited combinations, the present work unifies these physical phenomena into a single transient framework, thereby providing a more realistic representation of coupled heat and mass transfer processes encountered in advanced engineering systems.

## RESEARCH SIGNIFICANT

This study makes important theoretical, computational, and practical contributions to the field of heat and mass transfer involving hybrid nanofluids. By developing a comprehensive transient magnetohydrodynamic (MHD) model for Ag–Cu/water hybrid nanofluid flow over an inclined porous plate with thermal radiation, heat generation/absorption, chemical reaction, and Soret-Dufour effects, the research enhances the understanding of complex transport phenomena encountered in advanced thermal engineering applications. The study expands the existing body of knowledge on hybrid nanofluid transport by investigating the simultaneous interaction of multiple physical mechanisms that have largely been studied independently in previous research. The comprehensive analysis of these coupled effects provides a deeper understanding of the relationships among momentum, heat, and mass transfer in electrically conducting hybrid nanofluids, thereby serving as a valuable reference for future theoretical and numerical investigations.

**Model description**

This study considers the transient magnetohydrodynamic (MHD) free-convective transport of an electrically conducting Ag–Cu/water hybrid nanofluid over an infinitely long, inclined porous plate embedded in a saturated porous medium. Firstly, the plate is at zero velocity with the ambient temperature. At times, the plate begins to change position in its own plane with upward velocity, and its temperature rises or falls. We select the axis along the plate in the upward-inclined direction and the axis perpendicular to the plate. An undeviating transverse magnetic field of strength is employed parallel to the axis. The plate matches the plane, and the flow is restricted to. The physical model of the flow is illustrated in Figure 1. The assumptions of the present problem are as follows. The pressure gradient is neglected in this problem. A radiative heat flux is introduced in the normal direction to the plate. The fluid is a water-based nanofluid comprising two types of nanoparticles. The base fluid and the mixed nanoparticles are in thermal balance. The density is assumed to be linearly dependent on temperature and buoyancy forces in the equations of motion. This approximation is sufficiently accurate for drops and gases at small temperature differences. A uniform transverse magnetic field of strength B0is applied perpendicular to the direction of flow. Because the magnetic Reynolds number is sufficiently small, the magnetic field induced by fluid motion is neglected compared with the applied magnetic field. Likewise, no externally imposed electric field is present, and Hall current, ion slip, Joule heating, viscous dissipation, and electric polarization effects are assumed to be negligible. These assumptions are commonly adopted in low-magnetic-Reynolds-number MHD flows and considerably simplify the mathematical formulation without compromising physical realism, as noted in [Mahanthesh *et al*, (2016), Arshad *et al* (2021)].

$$\rho_{nf}\frac{\partial v'}{\partial \tau'}=\mu_{nf}\frac{\partial^2 v'}{\partial z'^2}-\sigma_{nf}B_0^2 v'+\frac{\mu_{nf}\phi^*}{k}v'+g(\rho B_1)_{nf}(\theta'-\theta_\infty')(\cos\alpha)+g(\rho\beta_2)_{nf}(\phi'-\phi_\infty')(\cos\alpha)$$

(1)

$$\frac{\partial C_1}{\partial t_1}+u'\frac{\partial C_1}{\partial x_1}+v'\frac{\partial C_1}{\partial y_1}=D_{nf}\frac{\partial^2 C_1}{\partial {y_1}^2}-\gamma^c(C_1'-C_{1\infty}')+\frac{D_m k_T}{T_m}\frac{\partial^2 T_1}{\partial {y_1}^2}$$

(2)

$$\frac{\partial \phi'}{\partial \tau'}=D_{nf}\frac{\partial^2 \phi'}{\partial z'^2}-k_r'(\phi'-\phi_\infty')+\frac{D_m k_T}{T_m}\frac{\partial^2 \phi'}{\partial z'^2}$$

(3)

Where

$v',\theta',\phi',\rho_{nf},\mu_{nf},\sigma_{nf},(\rho B_1)_{nf},(\rho\beta_2)_{nf},g,\phi^*,Q^*,(\rho C_p)_{nf},k_{nf},D_{nf},k_r',D_m,T_m,k_T,\alpha$ is fluid velocity, nanofluid temperature, nanofluid concentration, nanofluid density, dynamic viscosity of nanofluid, electrical conductivity of nanofluids, thermal expansion coefficient, coefficient of volumetric expansion, acceleration due to gravity, porosity of the porous medium, heat absorption constant, specific heat capacity of the nanofluid, thermal conductivity, of nanofluid, mass diffusivity, chemical reaction parameter, chemical molecular diffusivity, thermal diffusion rate, and inclination angle respectively.

And the characteristic time $t_0$ is defined as $\tau_0=\frac{v_f}{U_0^2}$

For nanofluids, the parameters $\rho_{nf},\mu_{nf},(\rho c_p)_{nf},(\rho B_T)_{nf},(\rho\beta_c)_{nf},\sigma_{nf}$ are

https://dx.doi.org/10.4314/swj.v21i3.10

demarcated as [8,11]:

$$\rho_{nf}=(1-\phi)\rho_f+\phi\rho_s,\ \mu_{nf}=\frac{\mu_f}{(1-\phi)^{2.5}},\ (\rho c_p)_{nf}=(1-\phi)(\rho c_p)_f+\phi(\rho c_p)_s,$$

$$(\rho B_T)_{nf}=(1-\phi)(\rho B_T)_f+\phi(\rho B_T)_s,\ \sigma_{nf}=\sigma_f\left(1+\frac{3(\sigma-1)\phi}{(\sigma+2)-(\sigma-1)\phi}\right)\ \text{where } \sigma=\frac{\sigma_f}{\sigma_s},$$

$$\frac{k_{nf}}{k_f}=\frac{k_s+2k_f-2\phi(k_f-k_s)}{k_s+2k_f+\phi(k_f-k_s)},$$

Where

$\phi,\rho_f,\rho_s,\sigma_f,\sigma_s,\mu_f,(\rho c_p)_f,(\rho c_p)_s,k_f,k_s$ is the nanoparticle volume fraction, density of the base fluid, density of the nanoparticles, electrical conductivity of the base fluid, electrical conductivity of the nanoparticles, viscosity of the base fluid, heat capacitance of the base fluid, heat capacitance of the nanoparticles, thermal conductivity of the base fluid, and thermal conductivity of the nanoparticles, respectively.

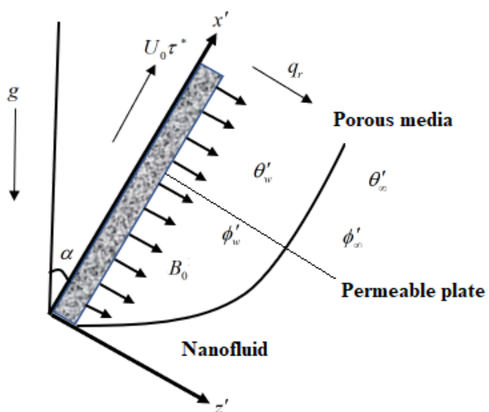


**Figure 1**: Illustrative sketch of the model

The appropriate initial and boundary conditions flow are as provided in [Hayat *et al* (2017), Balla *et al* (2020), Shamshuddin *et al* (2021), Puneeth *et al* (2021) and Arshad *et al* (2021)];

$$\left.\begin{array}{llll} v'=0,\ \theta'=\theta'_\infty,\ \phi'=\phi'_\infty & \text{for all } z' & \text{and} & \tau'\le 0 \\ u'=U_0\tau^*,\ \theta'=\theta'_w,\ \phi'=\phi'_w & \text{at}\quad z'=0 & \text{for} & \tau'>0 \\ u'\to 0,\ w'\to 0,\ \theta'\to\theta'_w,\ \phi'=\phi'_w & \text{as}\quad z'\to\infty & \text{for} & \tau'>0 \end{array}\right\}$$

(4)

The Rosseland approximation applies to optically thick media and gives the net radiation heat flux $q_r$ through the expression as in [Shamshuddin *et al* (2021), Kumar *et al* (2021)],

$$q_r=-\frac{4\sigma'}{3k'}\frac{\partial\theta'^4}{\partial z'}$$

(5)

where $\sigma'$ and $k'$ denote, respectively, the Stefan-Boltzmann constant and absorption coefficient. It is assumed that the temperature difference within the boundary-layer flow is sufficiently small that the term $\theta'^4$ may be expressed as a linear function of temperature. This is done by expanding $\theta'^4$ in a Taylor series about a free stream temperature $\theta_\infty{}'$ as pursues

$$\theta'^4=\theta_\infty'^4+3\theta_\infty'^3(\theta'-\theta'_\infty)+6\theta_\infty'^2(\theta'-\theta'_\infty)^2+\ldots \quad (6)$$

Neglecting higher-order terms in Eq. (6) ahead of the first order in $(\theta'-\theta'_\infty)$, we attain,

$$\theta'^4\cong 4\theta_\infty'^3\theta'-3\theta_\infty'^4$$

(7)

Differentiating equation (7) with respect to $z'$ we obtain

$$\frac{\partial\theta'^4}{\partial z'}=4\theta_\infty'^3\frac{\partial\theta'}{\partial z'}$$

(8)

Now substitute equation (8) into equation (5)

$$q_r=-\frac{4\sigma'}{3k'}\left(4\theta_\infty'^3\frac{\partial\theta'}{\partial z'}\right)=-\frac{16\sigma'\theta_\infty'^3}{3k'}\frac{\partial\theta'}{\partial z'}$$

(9)

Differentiating $q_r$ with respect to $z'$ one acquires

$$\frac{\partial q_r}{\partial z'}=-\frac{16\sigma'\theta_\infty'^3}{3k'}\frac{\partial^2\theta'}{\partial z'^2}$$

(10)

Substituting equation (10) into equation (2) results

$$\frac{\partial\theta'}{\partial\tau'}=\frac{k_{nf}}{(\rho c_p)_{nf}}\frac{\partial^2\theta'}{\partial z'^2}-\frac{1}{(\rho c_p)_{nf}}\left(k_{nf}+\frac{16\sigma'\theta_\infty'^3}{3k'}\right)\frac{\partial^2\theta'}{\partial z'^2}-\frac{1}{(\rho c_p)_{nf}}Q^*(\theta'-\theta_\infty{}')+\frac{D_m k_T}{c_s c_p}\frac{\partial^2\phi'}{\partial z'^2}$$

(11)

Introducing dimensionless parameters

$$\left.\begin{array}{l} v=\frac{v'}{U_0},z=\frac{U_0 z'}{v_f},\tau=\frac{U_0^2\tau'}{v_f},\theta=\frac{\theta'-\theta'_\infty}{\theta'_w-\theta_\infty{}'},C=\frac{\phi'-\phi'_\infty}{\phi'_w-\phi'_\infty},M^2=\frac{\beta_3 v_f\sigma_f B_0^2}{\rho_{nf}U_0^2},R=\frac{16\sigma_1 T_\infty'^3}{3kk^*}, \\ K_1=\frac{kU_0^2}{v_{nf}\phi^* v_f},P_r=\frac{(\mu c_p)_f}{k_f},G_r=\frac{v_f g\beta_{1Tf}(\theta'_w-\theta_\infty{}')}{U_0^3},G_m=\frac{v_f g\beta_{2f}(\phi'_w-\phi'_\infty)}{U_0^3},S_c=\frac{v_f}{D_{nf}}, \\ Q_s=\frac{v_f Q^*(\phi'_w-\phi'_\infty)}{U_0^2(\theta'_w-\theta_\infty{}')}\gamma=\frac{k'_r v_f}{U_0{}^2},S_r=\frac{D_m k_T(\theta'_w-\theta_\infty{}')}{v_f T_m(\phi'_w-\phi'_\infty)},D_u=\frac{D_m k_T}{vc_s c_p}\frac{(\phi'_w-\phi'_\infty)}{(\theta'_w-\theta_\infty{}')}, \end{array}\right\}$$

(12)

Utilizing dimensionless variables, the governing equations. (1), (3) and (11) reduce to

$$\frac{\partial v}{\partial\tau}=\frac{1}{R_e}\frac{\partial^2 v}{\partial z^2}-M^2 v-\frac{1}{K_1}v+y_1 G_T T(\cos\alpha)+y_2 G_C C(\cos\alpha),$$

(13)

$$\frac{\partial T}{\partial\tau}=\frac{1}{b_1}\left(\frac{1+R}{P_r}\right)\frac{\partial^2 T}{\partial z^2}+Q_1 T+D_u\frac{\partial^2 C}{\partial z^2}, \quad (14)$$

$$\frac{\partial C}{\partial\tau}=\frac{1}{S_c}\left(\frac{\partial^2 C}{\partial z^2}\right)+S_r\left(\frac{\partial^2 T}{\partial z^2}\right)-\gamma C \quad (15)$$

Where $R_e,M^2,P_r,G_T,G_C,S_c,K_1,R,Q_1,S_r,D_u$ Reynolds number, Magnetic field parameter, Prandtl number, thermal Grashof number, solutal Grashof number, Schmidt number, porosity parameter, thermal radiation parameter, dimensionless heat source parameter, Soret number, and Dufour number respectively.

Parameters and variables appearing in Eqs. (12-15) are defined as:

Science World Journal Vol. 21(No 3) 2026
www.scienceworldjournal.org
ISSN: 1597-6343 (Online), ISSN: 2756-391X (Print)
Published by Faculty of Science, Kaduna State University
https://dx.doi.org/10.4314/swj.v21i3.10

$$R_e = (1-\phi)^{2.5}\left[(1-\phi)+\phi\left(\frac{\rho_s}{\rho_f}\right)\right],\quad b_1=\frac{\beta_4}{\lambda_{nf}},\quad \lambda_{nf}=\frac{k_{nf}}{k_f},$$

$$y_1=\frac{(1-\phi)\rho_f-\phi\rho_s\left(\frac{\beta_{1s}}{\beta_{1f}}\right)}{\rho_{nf}},\quad y_2=\frac{(1-\phi)\rho_f-\phi\rho_s\left(\frac{\beta_{2s}}{\beta_{2f}}\right)}{\rho_{nf}}$$

$$\beta_3=1+\frac{3(\sigma-1)\phi}{(\sigma+2)-(\sigma-1)\phi},\quad \beta_4=(1-\phi)+\phi\left(\frac{(\rho c_p)_s}{(\rho c_p)_f}\right)$$

The consistent initial and boundary conditions in the dimensionless form are specified as [Hayat *et al* (2017), Balla *et al* (2020), Shamshuddin *et al* (2021)]:

$$\left.\begin{array}{llll}\tau\le 0; & v=0, & T=0,\ C=0, & \text{for all } z\\ \tau>0; & v=\tau^*, & T=1,\ C=1, & \text{at } z=0\\ v\to 0; & T\to 0, & C\to 0, & \text{as } z\to\infty\end{array}\right\}$$

(16)

The thermal-physical properties of base fluid and nanoparticles are portrayed in Table 1, following Shamshuddin *et al* (2021).

**Table 1**. Thermal-physical properties of nanofluids

| | $H_2O$ | $Ag$ | $Cu$ |
|---|---|---|---|
| $c_p(kg^{-1}K^{-1})$ | 4179 | 235 | 385 |
| $\rho(kgm^{-3})$ | 997.1 | $1.05\times10^4$ | 8933 |
| $k(Wm^{-1}K^{-1})$ | 0.613 | 429 | 401 |
| $\beta\times10^{-5}(K^{-1})$ | 21 | 1.89 | 1.67 |
| $\sigma(S/m)$ | $5.5\times10^{-6}$ | $62.1\times10^6$ | $5.9.6\times10^6$ |

With considerable physical engineering properties analogous to thermal and solutal flow potentials encompassing the wall-friction coefficient $\tau_x$, heat and mass transfer rates in terms of the Nusselt number $N_u$, and Sherwood number $S_h$, which are described in dimensionless form by

$$C_f=\left(\frac{\partial v}{\partial z}\right)_{z=0},\ N_u=\left(\frac{\partial T}{\partial z}\right)_{z=0} \text{ and}$$

$$S_h=\left(\frac{\partial C}{\partial z}\right)_{z=0}.. \qquad (17)$$

**3. Computation scheme methodology**

The coupled quasi-linear PDEs, $(13)-(15)$ collectively with initial and boundary regulations, Eqs. represent the flow-determining equations of the proposed model. The analytical (exact) solutions to the equations mentioned are almost impossible to obtain. Thus, the explicit finite-difference scheme is used to solve Eqs along with Eqs. $(16)$. This solution methodology is employed because of its suitability, consistency, stability and convergence. The forward time central in space for $v, T$ and $C$ is given as follows:

$$\left.\begin{array}{l}\dfrac{\partial v}{\partial\tau}=\dfrac{v_{i,j+1}-v_{i,j}}{\Delta\tau},\ \dfrac{\partial T}{\partial\tau}=\dfrac{T_{i,j+1}-T_{i,j}}{\Delta\tau},\ \dfrac{\partial C}{\partial\tau}=\dfrac{C_{i,j+1}-C_{i,j}}{\Delta\tau}\\ \dfrac{\partial v}{\partial z}=\dfrac{v_{i+1,j}-v_{i-1,j}}{2\Delta z},\ \dfrac{\partial T}{\partial z}=\dfrac{T_{i+1,j}-T_{i-1,j}}{2\Delta z},\ \dfrac{\partial C}{\partial z}=\dfrac{C_{i+1,j}-C_{i-1,j}}{2\Delta z}\\ \dfrac{\partial^2 v}{\partial z^2}=\dfrac{v_{i-1,j}-2v_{i,j}+v_{i+1,j}}{(\Delta z)^2},\ \dfrac{\partial^2 T}{\partial z^2}=\dfrac{T_{i-1,j}-2T_{i,j}+T_{i+1,j}}{(\Delta z)^2},\\ \dfrac{\partial^2 C}{\partial z^2}=\dfrac{C_{i-1,j}-2C_{i,j}+C_{i+1,j}}{(\Delta z)^2},\ v=v_{i,j},\ T=T_{i,j},\ C=C_{i,j}.\end{array}\right\}$$

Substituting Eqs. $(14)$ and $(15)$ into Eqs. $(11)-(12)$ yields the following governing equation in finite difference form: -

$$\frac{v_{i,j+1}-v_{i,j}}{\Delta\tau}=\frac{1}{R_e}\left(\frac{v_{i-1,j}-2v_{i,j}+v_{i+1,j}}{(\Delta z)^2}\right)-M^2v_{i,j}-\frac{1}{K_1}v_{i,j}+y_1G_TT_{i,j}(\cos\alpha)+y_2G_CC_{i,j}(\cos\alpha),$$

(18)

$$\frac{T_{i,j+1}-T_{i,j}}{\Delta\tau}=\frac{1}{b_1}\left(\frac{1+R}{P_r}\right)\left(\frac{T_{i-1,j}-2T_{i,j}+T_{i+1,j}}{(\Delta z)^2}\right)+Q_1T_{i,j}+D_u\left(\frac{C_{i-1,j}-2C_{i,j}+C_{i+1,j}}{(\Delta z)^2}\right),$$

(19)

$$\frac{C_{i,j+1}-C_{i,j}}{\Delta\tau}=\frac{1}{S_c}\left(\frac{C_{i-1,j}-2C_{i,j}+C_{i+1,j}}{(\Delta z)^2}\right)+S_r\left(\frac{T_{i-1,j}-2T_{i,j}+T_{i+1,j}}{(\Delta z)^2}\right)-\gamma C_{i,j}$$

(20)

Subjected to the transformed initial and boundary conditions:

$$\left.\begin{array}{llll}\tau\le 0; & v_{i,j}=0, & T_{i,j}=0,\ C_{i,j}=0, & \text{for all } i \text{ and } j\\ \tau>0; & v_{i,j}=\tau^*, & T_{i,j}=1,\ C_{i,j}=1, & \text{at } i=0 \text{ for } j>0\\ v_{i,j}\to 0; & T_{i,j}\to 0, & C_{i,j}\to 0, & \text{as } i\to\infty \text{ for } j>0\end{array}\right\}$$

(21)

The computation scheme is carried out using the adopted default values $Re=0.2,\ M=0.5,\ K_1=0.3,\ \alpha=\pi/4, Gr=0.3,$ $Gc=0.3,\ R=0.7,\ Pr=7.0,\ Q_1=2.0,\ Du=0.3,\ Sr=0.6,\ Sr=0.4,\ \gamma=1.0$. These baseline values were adopted from previously published studies to facilitate meaningful comparison with existing results. To establish the accuracy and reliability of the proposed numerical scheme, the present results are validated against those reported by Gopal *et al* (2023) and Das & Jana (2015) for a reduced version of the governing model obtained by suppressing selected physical effects. As shown in Table 2, the computed results agree well with the published data, with negligible numerical discrepancies attributable to computational precision. This close correspondence confirms the correctness, stability, and robustness of the explicit finite difference algorithm employed in the present study and provides confidence in the subsequent parametric analysis.

https://dx.doi.org/10.4314/swj.v21i3.10

**Table 2:** Results validation when $Gc = 0, \alpha = \frac{\pi}{2}, Du = 0, Sr = 0, \gamma = 0, y_1 = 1, \tau * = 0$

| K | $\phi$ | R | M | Gopal *et al.* [25] | Das and Jana [31] | Present |
|---|---|---|---|---|---|---|
| **0.5** | 0.05 | 1.0 | 2.0 | 0.522145 | 0.522142 | 0.52214477 |
| | | | 3.0 | 0.458496 | 0.458448 | 0.45846824 |
| | | | 4.0 | 0.355447 | 0.355487 | 0.35548384 |
| **1.0** | | | | 0.565852 | 0.565894 | 0.56589283 |
| **1.5** | | | | 0.605241 | 0.605221 | 0.60522083 |
| | | 1.5 | | 0.587463 | 0.587447 | 0.58744358 |
| | | 2.0 | | 0.622447 | 0.622465 | 0.62246182 |
| | 0.20 | | | 0.597996 | 0.597995 | 0.59799428 |
| | 0.40 | | | 0.650621 | 0.650632 | 0.65063128 |

**RESULTS AND DISCUSSION**

Figure 2 illustrates the influence of the porosity parameter ($K_1$) on the velocity profile of the Ag-Cu/water hybrid nanofluid at two time levels, $\tau^* = 0.5$ and $\tau^* = 1.0$. It is observed that increasing ($K_1$) significantly reduces the fluid velocity throughout the boundary layer. Physically, a larger porosity parameter corresponds to greater resistance from the porous medium, which opposes fluid motion and suppresses momentum transport. Consequently, the momentum boundary layer becomes thinner as ($K_1$) increases. Furthermore, the velocity profiles at $\tau^* = 1.0$are higher than those at $\tau^* = 0.5$, indicating that the flow develops and accelerates with time. Figure 3 depicts the variation of velocity with the thermal Grashof number (Gr). The velocity increases markedly as (Gr) increases from 0.5 to 5.0. Since (Gr) measures the ratio of buoyancy forces to viscous forces, larger values enhance thermal buoyancy generated by temperature differences between the plate and the ambient fluid. The strengthened buoyancy force accelerates the fluid particles adjacent to the heated plate, resulting in thicker momentum boundary layers and higher flow velocities. This behaviour confirms the dominant role of thermal convection in enhancing fluid transport. The influence of the solutal Grashof number (Gc) on the velocity field is presented in Figure 4. An increase in (Gc) substantially enhances the fluid velocity. Physically, (Gc) quantifies the contribution of concentration-induced buoyancy forces. Higher concentration gradients generate stronger buoyancy effects, which aid fluid motion and increase the thickness of the momentum boundary layer. Therefore, the combined action of thermal and concentration buoyancy significantly promotes convective transport within the flow region.

Figure 5 demonstrates the impact of the thermal radiation parameter (R) on the temperature distribution. The temperature profile increases appreciably with increasing values of (R). This behaviour occurs because thermal radiation contributes additional energy to the fluid, thereby increasing its thermal content. The enhanced radiative heat transfer thickens the thermal boundary layer and slows the rate of temperature decay from the plate. Consequently, fluids exposed to stronger radiative effects maintain higher temperatures throughout the flow domain. Figure 6 presents the thermal response of the hybrid nanofluid for various values of the heat source parameter ( $Q_1$ ). It is evident that increasing ( $Q_1$ ) elevates the fluid temperature and significantly enlarges the thermal boundary layer. Physically, larger values of ( $Q_1$ ) indicate greater internal heat generation in the fluid, thereby supplying additional thermal energy and enhancing molecular activity. As a result, heat diffusion from the plate becomes more pronounced, leading to higher temperature levels throughout the fluid region. The influence of the Dufour number (Du) on the temperature field is illustrated in Figure 7. Increasing (Du) results in a notable rise in temperature and thermal boundary layer thickness. The Dufour effect represents heat transfer induced by concentration gradients. Therefore, larger values of (Du) increase the amount of energy transported from species diffusion into the thermal field, generating additional heat within the fluid. This cross-diffusion mechanism enhances thermal transport and elevates the overall temperature distribution.

Figure 8 displays the concentration profiles for different values of the Soret number (Sr)—the concentration distribution increases as (Sr) increases. Physically, the Soret effect describes mass transport induced by temperature gradients. Stronger thermal diffusion drives more species from higher- to lower-temperature regions, thereby increasing species accumulation within the boundary layer. Consequently, the concentration boundary layer becomes thicker with increasing (Sr), demonstrating the significant coupling between thermal and mass diffusion processes. Figure 9 illustrates the effect of the Schmidt number (Sc) on the concentration field. The concentration profile decreases as (Sc) increases from 0.2 to 1.0. Since (Sc) is the ratio of momentum diffusivity to mass diffusivity, larger values correspond to lower molecular diffusivity. Reduced mass diffusion weakens species transport away from the plate, thereby shrinking the concentration boundary layer. Therefore, higher Schmidt numbers lead to lower concentration levels throughout the fluid domain. Figure 10 shows the influence of the chemical reaction parameter (γ) on species concentration. It is observed that increasing (γ)significantly reduces the concentration profile. Physically, stronger chemical reactions accelerate the consumption of diffusing species, thereby reducing species concentration within the boundary layer. The resulting depletion of reactant species weakens mass transport and produces a thinner concentration boundary layer. This behaviour is characteristic of destructive chemical reactions that remove species from the flow system.

Figure 11 presents the variation of the skin-friction coefficient ($C_f$) with the magnetic parameter (M) for different values of (Gr). The magnitude of the skin friction decreases as (Gr) increases. Higher thermal buoyancy assists fluid motion and reduces the velocity gradient at the wall, thereby lowering the wall shear stress. The figure also shows that increasing (M) increases the magnitude of wall drag due to the retarding Lorentz force generated by the magnetic field. Thus, magnetic effects tend to enhance wall resistance, whereas thermal buoyancy acts to reduce it. Figure 12 illustrates the variation of the Nusselt number (Nu) with the heat source parameter ($Q_1$) for different values of the Dufour number (Du). The Nusselt number increases significantly as both (Du) and ($Q_1$) increase. Since the Dufour effect provides additional thermal energy through concentration gradients, the resulting enhancement in wall-normal temperature gradients improves the

https://dx.doi.org/10.4314/swj.v21i3.10
ISSN: 1597-6343 (Online), ISSN: 2756-391X (Print)
Published by Faculty of Science, Kaduna State University

heat transfer. Similarly, internal heat generation intensifies thermal transport, leading to higher Nusselt numbers. These observations indicate that cross-diffusion effects can substantially enhance thermal performance in hybrid nanofluid systems.

Figure 13 depicts the variation of the Sherwood number (Sh) with the Soret number (Sr) for different values of the chemical reaction parameter (γ). The Sherwood number increases with increasing (γ). A stronger chemical reaction intensifies species consumption, thereby increasing the concentration gradient at the wall and enhances the mass transfer rate. Conversely, increasing (Sr) tends to reduce the magnitude of the Sherwood number because thermal diffusion promotes species accumulation within the boundary layer, thereby weakening the wall concentration gradient. Hence, chemical reaction effects enhance mass transfer, while thermal diffusion tends to moderate it.

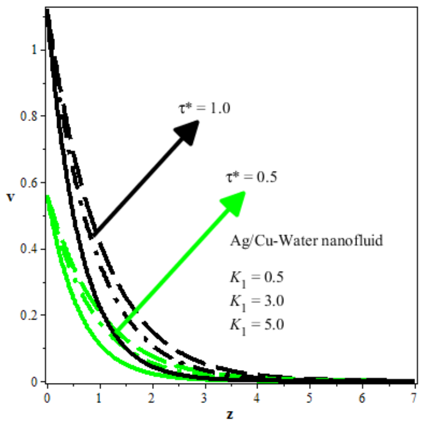


**Figure 2**: The effect of the porosity term on velocity

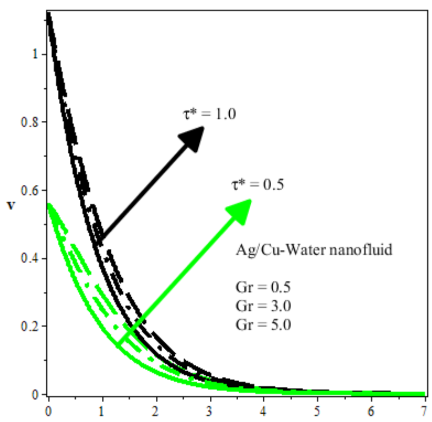


**Figure 3**: Impact of Gr on the flow velocity

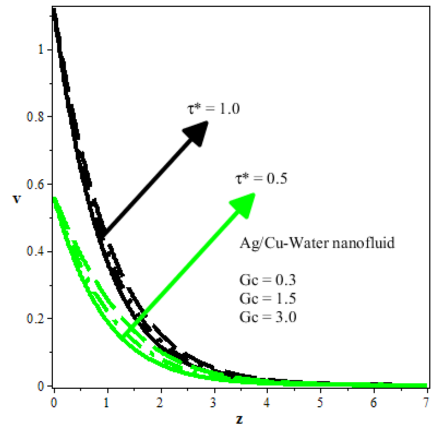


**Figure 4:** Influence of Gcon the velocity field

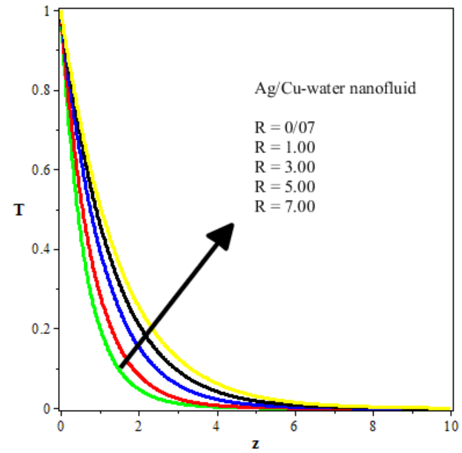


**Figure 5**: Temperature field for increasing R

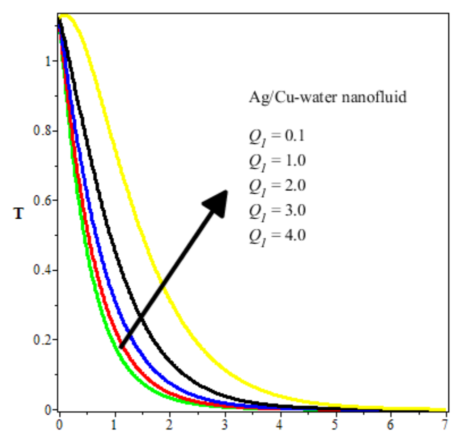


**Figure 6**: Thermal distribution for various $Q_1$

*ISSN: 1597-6343 (Online), ISSN: 2756-391X (Print)*
*Published by Faculty of Science, Kaduna State University*
https://dx.doi.org/10.4314/swj.v21i3.10

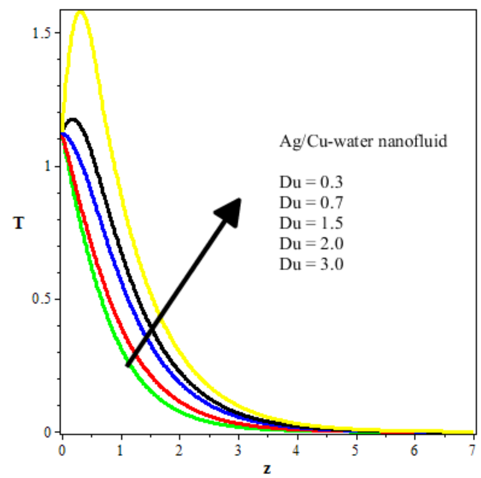


**Figure 7:** Heat profile for rising Dufour number

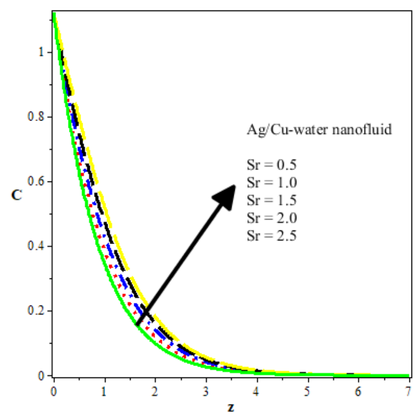


**Figure 8**: Mass transfer for different Sr

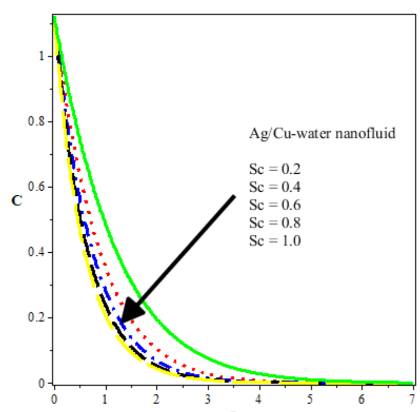


**Figure 9:** Concentration field for rising Sc

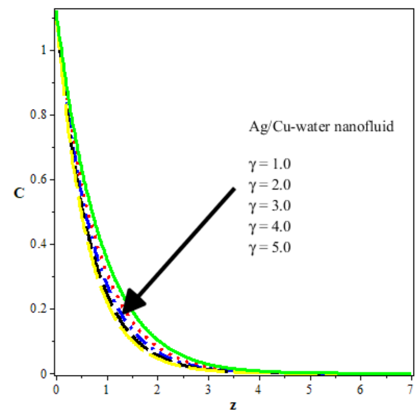


**Figure 10**: Species field for chemical reaction term

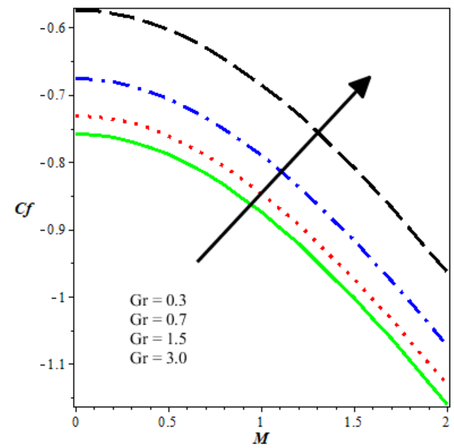


**Figure 11:** Skin friction for different Gr

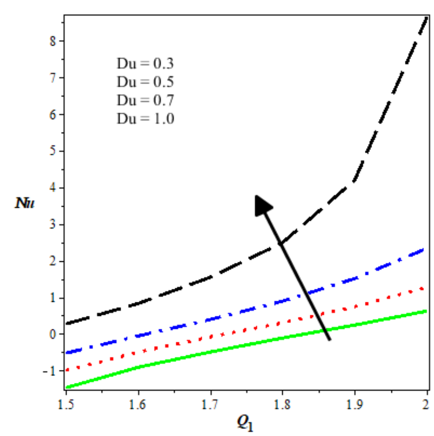


**Figure 12:** Nusselt number profile for various Du

https://dx.doi.org/10.4314/swj.v21i3.10

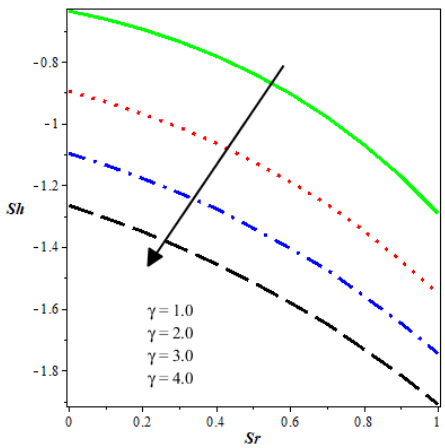


**Figure 13**: Chemical reaction on Sherwood number

**Conclusion**

This study presented a numerical investigation of the transient magnetohydrodynamic (MHD) double-diffusive free convective flow of an Ag-Cu/water hybrid nanofluid over an inclined porous plate, accounting for thermal radiation, heat generation, chemical reaction, and Soret–Dufour cross-diffusion effects. The governing momentum, energy, and concentration equations were transformed to dimensionless form and solved using an explicit finite-difference scheme. The major findings are summarized as follows.

1) Increasing the porosity parameter reduced the fluid velocity by increasing the porous medium's hydrodynamic resistance.
2) Larger thermal and solutal Grashof numbers enhanced buoyancy forces and significantly accelerated the fluid flow.
3) Thermal radiation, heat generation, and the Dufour effect increased the temperature distribution and thickened the thermal boundary layer.
4) The Soret effect enhanced the concentration of the species by promoting thermal diffusion.
5) Higher Schmidt numbers and stronger chemical reactions reduced the concentration boundary layer by decreasing mass diffusivity and increasing species consumption.
6) Stronger chemical reactions increased the Sherwood number, demonstrating enhanced mass transfer at the plate surface.

The present model provides a useful framework for analyzing coupled heat and mass transfer phenomena in hybrid nanofluids. Future work may extend the analysis by incorporating non-Newtonian hybrid nanofluids, variable thermophysical properties, nonlinear thermal radiation, or fractional-order formulations to capture memory effects in transient transport processes.

**REFERENCES**

Arshad, M., Hussain, A., Hassan, A., Haider, Q., Ibrahim, A. H., Alqurashi, M. S., & Abdussattar, A. (2021). Thermophoresis and Brownian motion effects in chemically reacting magnetohydrodynamic nanofluid flow across an exponentially stretching sheet. *Energies*, *15*(1), Article 143.

Azmi, H., Abdul Hamid, K., Mamat, R., & Sharma, K. V. (2016). Effects of working temperature on the thermo-physical properties and forced-convection heat transfer of TiO2 nanofluids in a water-ethylene glycol mixture. *Applied Thermal Engineering*, *106*, 1190–1199.

Balla, C. S., Alluguvelli, R., Naikoti, K., & Makinde, O. D. (2020). Effect of chemical reaction on bioconvective flow in oxytactic microorganisms suspended in a porous cavity. *Journal of Applied and Computational Mechanics*, *6*(3), 653–664.

Biswas, R., Hossain, M. S., Islam, R., Ahmmed, S. F., Mishra, S. R., & Afikuzzaman, M. (2022). Computational treatment of MHD Maxwell nanofluid flow across a stretching sheet considering higher-order chemical reaction and thermal radiation—Journal *of Computational Mathematics and Data Science*, *4*, Article 100048.

Choi, S. U. S. (1995). Enhancing thermal conductivity of fluids with nanoparticles. In D. A. Siginer & H. P. Wang (Eds.), *Developments and applications of non-Newtonian flows* (FED-Vol. 231/MD-Vol. 66, pp. 99–105)—American Society of Mechanical Engineers.

Das, S., & Jana, R. N. (2015). Natural convective magneto-nanofluid flow and radiative heat transfer past a moving vertical plate. *Alexandria Engineering Journal*, *54*(1), 55–64.

Gopal, H. K., Sundhakar, M., & Masthan Rao, S. (2023). Unsteady Magnetohydrodynamics (MHD) natural convective flow of nanofluids over an infinite perpendicular absorbent plate. *Journal of Nanofluids*, *12*(1), 280–287.

Haritha, A., Vishali, B., & Venkata Lakshmi, C. (2023). Heat and mass transfer of MHD Jeffrey nanofluid flow through porous media past an inclined plate with chemical reaction, radiation, and Soret effects. *Heat Transfer*, *52*(2), 1178–1197.

Hayat, T., & Nadeem, S. (2017). Heat transfer enhancement with Ag–CuO/water hybrid nanofluid. *Results in Physics*, *7*, 2317–2324.

Hong, K. S., Hong, T.-K., & Yang, H.-S. (2006). Thermal conductivity of Fe nanofluids as a function of nanoparticle cluster size: Applied *Physics Letters*, *88*(3), Article 033106.

Khan, W. A., & Pop, I. (2010). Boundary layer flow of a nanofluid past a stretching sheet. *International Journal of Heat and Mass Transfer*, *53*(11–12), 2477–2483.

Kumar, M. A., Reddy, Y. D., Rao, V. S., & Goud, B. S. (2021). Thermal radiation impact on MHD heat transfer of a natural-convective nanofluid flow over an impulsively started vertical plate. *Case Studies in Thermal Engineering*, *24*, Article 100826.

Lee, S., Choi, S. U. S., Li, S., & Eastman, J. A. (1999). Measuring thermal conductivity of fluids containing oxide nanoparticles. *ASME Journal of Heat Transfer*, *121*(2), 280–288.

Mahanthesh, B., Gireesha, B. J., Gorla, R. S. R., Abbasi, F. M., & Shehzad, A. (2016). Numerical solutions for magnetohydrodynamic nanofluid flow over a bidirectional nonlinear stretching surface with a prescribed surface heat flux boundary condition. *Journal of Magnetism and Magnetic Materials*, *417*, 189–196.

Mustafa, M., Khan, J. A., Hayat, T., & Alsaedi, A. (2015). Boundary-layer flow of a nanofluid over a nonlinearly stretching sheet with a convective boundary condition. *IEEE Transactions on Nanotechnology*, *14*(1), 159–168.

Padmaja, K., & Rushi Kumar, B. (2022). Dufour and Soret effects on MHD flow of Cu-water and Al2O3-water nanofluid flow over a permeable rotating cone. In *Fuzzy Mathematical Analysis and Advances in Computational Mathematics* (pp. 221–236). Springer Singapore.

Puneeth, V., Manjunatha, S., Makinde, O. D., & Gireesha, B. J. (2021). Bioconvection of a radiating hybrid nanofluid past a thin needle in the presence of heterogeneous–homogeneous chemical reaction. *Journal of Heat Transfer*, *143*(4), Article 042502.

Raghunath, K. (2023). Study of heat and mass transfer of an unsteady magnetohydrodynamic nanofluid flow past a vertical porous plate in the presence of chemical reaction, radiation and Soret effects. *Journal of Nanofluids*, *12*(3), 767–776.

Reddy, Y. D., & Goud, B. S. (2023). Comprehensive analysis of the impact of thermal radiation on unsteady MHD nanofluid flow across an infinite vertical flat plate with ramped temperature and heat consumption. *Results in Engineering*, *17*, Article 100796.

Reddy, Y. D., Goud, B. S., Chamkha, A. J., & Kumar, M. A. (2022). Influence of radiation and viscous dissipation on MHD heat transfer Casson nanofluid flow along a nonlinear stretching surface with chemical reaction. *Heat Transfer*, *51*(4), 3495–3511.

Roja, A., & Gireesha, B. J. (2020). Impact of Hall and Ion effects on MHD couple stress nanofluid flow through an inclined channel subjected to convective, hydraulic slip, heat generation, and thermal radiation. *Heat Transfer*, *49*(6), 3314–3333.

Salawu, S. O., Obalalu, A. M., Fatunmbi, E. O., & Shamshuddin, M. D. (2023). Elastic deformation of thermal radiative and convective hybrid SWCNT-Ag and MWCNT-MoS4 magneto-nanofluids flow in a cylinder. *Results in Materials*, *17*, Article 100380.

Shamshuddin, M. D., Abderrahmane, A., Koulali, A., Eid, M. R., Shahzad, F., & Jamshed, W. (2021). Thermal and solutal performance of Cu/CuO nanoparticles on a non-linear radially stretching surface with heat source/sink and varying chemical reaction effects—International *Communications in Heat and Mass Transfer*, *129*, Article 105710.

Shamshuddin, M. D., Akkurt, N., Saeed, A., & Kumam, P. (2023). Radiation mechanism on dissipative ternary hybrid nanoliquid flow through a rotating disk encountered by Hall currents: HAM solution. *Alexandria Engineering Journal*, *65*, 543–559.

Shamshuddin, M. D., Shahzad, F., Jamshed, W., Bég, O. A., Eid, M. R., & Bég, T. A. (2023). Thermo-solutal stratification and chemical reaction effects on radiative magnetized nanofluid flow along an exponentially stretching sensor plate: Computational analysis. *Journal of Magnetism and Magnetic Materials*, *565*, Article 170286.

Siddique, I., Nadeem, M., Awrejcewicz, J., & Pawłowski, W. (2022). Soret and Dufour effects on unsteady MHD second-grade nanofluid flow across an exponentially stretching surface: Scientific *Reports*, *12*(1), Article 11811.

Singha, A. K., Seth, G. S., Bhattacharyya, K., Yadav, D., Verma, A. K., & Gautam, A. K. (2021). Soret and Dufour effects on hydromagnetic flow of H2O-based nanofluids induced by an exponentially expanding sheet saturated in a non-Darcian porous medium. *Journal of Nanofluids*, *10*(4), 506–517.

Sundar, L. S., Sharma, K. V., Singh, M. K., & Sousa, A. C. M. (2017). Hybrid nanofluids preparation, thermal properties, heat transfer and friction factor – a review. *Renewable and Sustainable Energy Reviews*, *68*, 185–198.

Suresh Kumar, Y., Hussain, S., Raghunath, K., Ali, F., Guedri, K., Eldin, S. M., & Khan, M. I. (2023). Numerical analysis of magnetohydrodynamics Casson nanofluid flow with activation energy, Hall current and thermal radiation. *Scientific Reports*, *13*(1), Article 4021.